Nanoscale

Accepted Manuscript

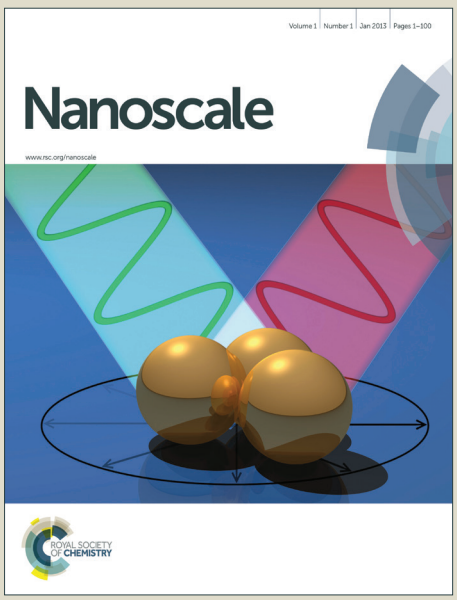

ROYAL SOCIETY OF CHEMISTRY

www.rsc.org/nanoscale

Journal Name

ARTICLE

2D Vanadium Doped Manganese Dioxides Nanosheets for Pseudocapacitive Energy Storage

Received 00th January 20xx,
Accepted 00th January 20xx

DOI: 10.1039/x0xx00000x

www.rsc.org/

Zhimi Hu‡[a], Xu Xiao‡[a], Liang Huang‡[a], Chi Chen[b], Tianqi Li[a], Tiecheng Su[a], Xiaofeng Cheng[a], Ling Miao[b], Yanrong Zhang[c] and Jun Zhou[a]*

Ultrathin two-dimensional (2D) crystals have been predicted to have high electrochemical activity in terms of nearly all active atoms are exposed to electrolyte, which offers great potential for energy storage. However, to construct layered structure metal oxides, it remains challenges that simplify the synthetic methods and improve the electronic conductivity. Here we synthesize 2D vanadium doped manganese oxides through a facile hydrothermal method. Vanadium dopant is also used as a template agent on the formation process of nanosheet-shaped MnO_2, further leading to high specific surface area as well as significant enhancement of the electronic conductivity which confirmed by the first principle calculations and four-point probe method. For the sake of shortened ion transport distance and enhanced electronic conductivity, V doped MnO_2 nanosheets display an excellent electrochemical performance as a supercapacitor electrode.

1. Introduction

By virtue of the excellent physical and chemical properties, environmental compatibility and high abundance, manganese dioxides (MnO_2) is deemed as a promising electrode material for energy storage. Among the varied crystal structures, α phase MnO_2 received special interest owing to its mesoporous channel structures formed by the stacking of MnO_6 octahedrons which would be beneficial to accessible ions transfer. [1,2] Nevertheless, the poor electrical conductivity (10^{-5}~10^{-6} S/cm) and significant performance degradation greatly confine the realization of its high theoretical capacitance (1370 F/g), especially at high charge/discharge rates and mass loading over 100 μg/cm^2, which hinder the commercialization of MnO_2 based energy storage devices.[3] To solve this problem, researchers have been focusing on engineering MnO_2 nanostructure to shorten the ion diffusion path or chemical modification to improve the electrical conductivity. For the former, various MnO_2 configurations ranging from zero-dimensional (0D) to three-dimensional (3D) nanostructured frameworks have been developed and tested in electrochemical capacitors (ECs).[4,5] Typically, as described by Brousse, and Devaraj, the two-dimensional (2D) MnO_2 based materials, comprised of edge-shared MnO_6 octahedra and the intercalated alkaline cations, is superior to one or three-dimensional crystals.[6-7] In terms of the layered structure, 2D MnO_2 could offer a unique opportunity to surpass the current limitations of electrode materials and achieved a high specific surface area to provide large electrochemically active surfaces. Recently, Zhu *et al.* synthesized ultrathin birnessite $K_{0.17}MnO_2$ nanosheets, of which the specific capacitance reached to 206 F/g at 1 A/g and decreased to 96 F/g at 10 A/g.[8] Zhao *et al.*, also presented the synthesis of MnO_2 nanosheets with a small quantity of K^+ ions in the interlayer. The specific capacitance rapidly decreased from 1017 F/g (3 mV/s) to 244 F/g (50 mV/s).[9] Although the high specific capacitance could be obtained from these layered structures, the low capacitance retention is still seinsfrage due to the poor electronic conductivity. Such a problem would be more obvious under high mass loading. For chemical modification, previous studies have shown that doping of heterogeneous elements into MnO_2 could improve the electronic conductivity, rendering a better performance in magnetic, electrical and electrochemical properties.[10-11] Moreover, impurities can be used to alter the properties of MnO_2 in desirable and controllable ways through careful selection of doping elements. Since electrochemical properties was extremely related to both active sites and electronic conductivity, simultaneously improving these two factors can synergistically enhance the ion diffusion and electron transport, leading to an excellent performance.

Herein, we demonstrate a hydrothermal method to design and modify 2D α-MnO_2 nanosheets with V doping. The first principle calculations revealed the possibility of the doping model: V-interstitial MnO_2. Doping with certain amount of V^{5+} not only efficiently enhance the conductivity of α-MnO_2, but

[a] Wuhan National Laboratory for Optoelectronics, and School of Optical and Electronic Information, Huazhong University of Science and Technology, Wuhan, 430074, China.
E-mail:jun.zhou@mail.hust.edu.cn
[b] School of Optical and Electronic Information, Huazhong University of Science and Technology, Wuhan 430074
[c] Environmental Science Research Institute, Huazhong University of Science and Technology, Wuhan 430074 (China)
‡ Authors with equal contribution
† Footnotes relating to the title and/or authors should appear here.
Electronic Supplementary Information (ESI) available: [details of any supplementary information available should be included here]. See DOI: 10.1039/x0xx00000x

also tailored the morphology from nanorods towards to nanosheets. Impressively, 2D V doped MnO_2 nanosheets display an excellent electrochemical performance with high specific capacitance of 439 F/g (195 F/cm^3 and 141 mF/cm^2) as well as excellent cycling stability (92 % maintained after 10,000 cycles).

2. Experimental Section

1) Synthesis of V doped MnO_2.

V doped MnO_2 was prepared by a hydrothermal method. $MnSO_4 \bullet H_2O$, $(NH_4)_2SO_4$ and $(NH_4)_2S_2O_8$ were added into 40 ml deionized water in a molar ratio 1: 2: 1. Different molar ratio of NH_4VO_3 were used as dopant reagents of vanadium in the above solution. Colourless solution was formed after stirring for about 10 minutes at room temperature. Then the solution transformed to a 50 ml stainless Teflon-lined autoclave and treated hydrothermally at 140 °C for 12 h. During reaction process, $MnSO_4$ was oxidized and turned to MnO_2. After filtration and washing several times by deionized water, the resulting precipitate was dried at 80 °C for 12 h, and then V doped α-MnO_2 was obtained. To investigate the influence of V doping, the different molar ratio 0.125:1, 0.25:1 and 0.5:1 of V^{5+} and Mn^{2+} in the initial solution were synthesized, and the products designated as 0.125 VMO, 0.25 VMO, and 0.5 VMO. And the pure MnO_2 for contrast was prepared by the same method named MO.

2) Preparation of the Electrodes.

Unless otherwise specified, the electrodes were composed of 70 wt.% MnO_2 powder, 30 wt.% CNT. After filtration and washing several times by deionized water, the resulting precipitate was dried at room temperature. Before electrochemical characterization, the electrodes were subsequently immersed in the electrolyte solution for 0.5 h in order to enhance the electrolyte diffusion into the material bulk.

3) Physical and Electrochemical Characterization.

The microstructural properties of electrode materials were characterized by X-ray diffraction using the Cu Kα radiation (λ=1.5418 Å) (XRD, Philips X' Pert Pro), field-emission SEM (FE-SEM, FEI Nova 450 Nano), TEM (HRTEM, TECNAI, Titan) equipped with an energy-dispersive X-ray spectroscopy (EDAX) detector, atomic force microscopy (AFM, SPM9700, Shimadzu), X-ray photoelectron spectroscope (XPS, AXIS-ULTRA DLD-600W). The electrochemical properties of the products were investigated with cyclic voltammetry (CV) and chronopotentiometry measurements employing EC-lab, and the electrochemical impedance spectroscopy (EIS) was measured by an Autolab PGSTAT302N at a frequency ranging from 100 mHz to 10 kHz with a potential amplitude of 10 mV. The mass of electrode materials were measured by a microbalance (CPA225D, Sartorius) with an accuracy of 0.01 mg. The element content of V was measured by inductively coupled plasma emission spectrum (ICP-OES, Optima 4300DV). N2 adsorption-desorption isotherms were performed on a Micrometrics ASAP 2000. Four-probe configuration electrical resistively was tested by a standard four-probe configuration (RTS-8) and the tested samples were prepared according the following process: Firstly, ~0.5 g V doped α-MnO_2 power was dried at 80 °C for 12 h; Then the power was pressed under a force of approximately 4 KPa by a table press machine (yp-180, Xingye). Infrared spectroscopy (IR) analysis of the materials was performed on a VERTEX 70 (Bruker) Fourier transformation infrared spectrometer over the wave number range of 400 ~ 4000 cm^{-1} with KBr pelletisation. Raman analysis was performed on a LabRAM HR800 (Horiba JobinYvon) with a 532 nm illuminant.

3. Results and Discussion

A facile hydrothermal method was used for the synthesis of V doped MnO_2 nanosheets and NH_4VO_3 was used as a dopant. To investigate the effects of V doping content, different amount of NH_4VO_3 were introduced from 0 mmol, 0.125 mmol, 0.25 mmol to 0.5 mmol, the related samples were denoted as MO, 0.125 VMO, 0.25 VMO and 0.5 VMO, respectively. The morphologies of V doped MnO_2 nanosheets were investigated by scanning electron microscopy (SEM), transmission electron microscopy (TEM) and atomic force microscopy (AFM). The pristine MnO_2 (MO) showed uniform nanorods structure under the same synthesis condition (Fig. S1). With less V dopant, nanobelts were obviously observed in 0.125 VMO and 0.25 VMO (Fig. S2). The layered structure of 0.5 VMO was clearly observed from the SEM and TEM measurements with the size exceeds 100 nm (Fig.1a, S3). The thickness of the nanosheets wasabout 1 nm to 3 nm (Fig. 1b). Such a difference revealed that V may efficiently tailor the morphology. The schematic of V doped MnO_2 synthesis process was given in Fig. 1c. The layered structure was constructed through merging of multiple single crystal MnO_2 nanosheets (Fig. S4a). Since the formation process mainly depended on the content of V dopant. The possible growth mechanism of V doped MnO_2 nanosheets can be divided into two stages: (I) The decomposition of NH_4VO_3 in acid solution to produce V_2O_5 layer structure; (II) MnO_2 was synthesized through the redox reaction between Mn^{2+} and $S_2O_8^{2-}$, (III) The decreased pH in solution results in the partial dissolution of V_2O_5 which could form a substrate to guide the growth of MnO_2 nanosheets and aggregate to MnO_2 layered structure following the deep dissolution of V_2O_5 phase. Accordingly, certain amount of V remain in layered structure along with the growth of MnO_2 nanosheets, resulting in the formation of 2D V doped MnO_2. When the V dopant exceeds 0.5 mmol, a mass of V_2O_5 sheets mixed with MnO_2 phase could be seen in SEM and EDS (Fig. S4b). This could verity our growth mechanism of V doped MnO_2 nanasheets. Figure 1d displayed the pale yellow dispersion solution of V doped MnO_2 nanosheets in ethanol and H_2O mixture solution (*v*: *v*= 3:7) without any precipitation when stored for three months. The existences of V element in three samples were detected by Energy-dispersive spectrum (EDS). From the element mapping of 0.5 VMO (Fig.1e), it can be seen that V was distributed uniformly in the sample and the intensity of V increased depending on the content of V (Fig. 1f). The actual content of the element V was further confirmed by different methods

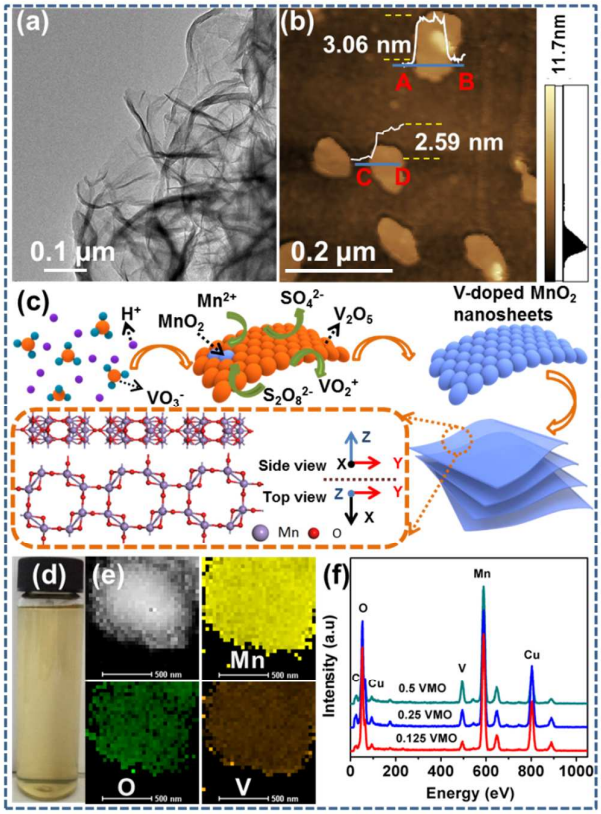

Fig. 1 Typical TEM (a) and AFM (b) image of 0.5 VMO. (c) Schematic for the synthesis of V doped MnO_2 nanosheets, and the insert shows the crystal structure of α-MnO_2 with (1 × 1) or (2 × 2) tunnels. (d) The dispersion solution of V doped MnO_2 nanosheets. (e) EDS mapping scanning of 0.5 VMO. (f) EDS of 0.5 VMO, 0.25 VMO, 0.125 VMO with normalized.

(Table S1). The content of V in 0.125 VMO, 0.25 VMO and 0.5 VMO were approximately 1.5 %, 2.5 % and 5.2 %, respectively.

In this work, a certain amount of V doping can significantly change the morphology of MnO_2. The specific surface area (SSA) of all samples was investigated and presented in Fig. 2a and Table S2. Undoubtedly, V doped MnO_2 nanosheets (0.5 VMO) has a specific surface area of 273 m^2/g, which is superior to 0.125 VMO (92 m^2/g), 0.25 VMO (151 m^2/g) and most of other reports about MnO_2 based materials.[7] Besides, the larger pore volume can also be obtained for V doped MnO_2 nanosheets (Table S2). Consequently, more active sites can be provided which would be beneficial to the electrochemical performance.

As the electrode materials for ECs, an important feature of MnO_2 is the presence of mesoporous channels formed by the stacking of MnO_6 octahedrons. β-MnO_2 has (1 × 1) tunnels, while α-MnO_2 has (2 × 2) and (1 × 1) tunnels by sharing the edges and corners of the MnO_6 octahedrons.[1] Lots of researches indicated that these tunnels structure would be advantageous to the electrochemical performance.[1,7] Fig. 2b showed the X-ray diffraction (XRD) patterns of V doped MnO_2. The XRD patterns clearly revealed the tetragonal phase α-MnO_2 (JCPDS 44-0141) of 0.125 VMO and 0.25 VMO. It should be noted that just two diffraction peaks at 37.3 ° and 66.8 ° were existed in 0.5 VMO. Hence the crystal structure should be further confirmed by other phase identification measurement. Raman scattering spectroscopy, affords useful alternatives or supplements to XRD for structural characterizations of materials. The sharp and high-frequency Raman bands of 0.5 VMO (Fig. 2c) at 637 cm^{-1} is indicative of a well-developed tetragonal structure with an interstitial space consisting of (2 × 2) tunnels, [12-13] implying the α-MnO_2 phase of this layered structure. Previous studies have shown that kinds of elements such as cations of alkaline, alkaline earth elements, as well as heavy metals can inset into the (2 × 2) tunnels to avoid the collapse and construct α phase MnO_2.[10] In our work, pure MnO_2 (MO) without addition of NH_4VO_3 is β-MnO_2 phase. This is a powerful evidence to prove that certain vanadium have inserted into the (2 × 2) tunnels to support the tunnels structure of α-MnO_2.

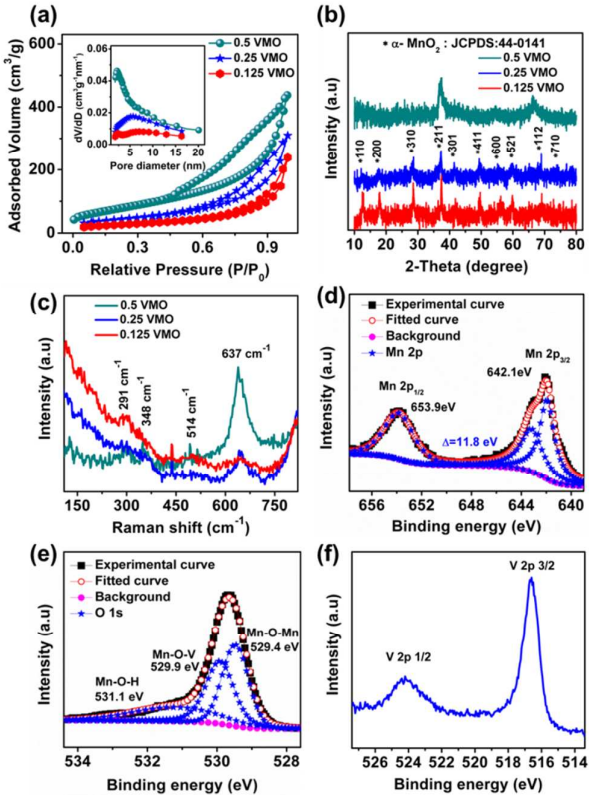

Fig. 2 (a) N_2-sorption isotherms of 0.5 VMO, 0.25 VMO, 0.125 VMO, the insert shows the pore distribution. (b) XRD patterns of 0.5 VMO, 0.25 VMO, 0.125 VMO. (c) Raman spectra of 0.5 VMO, 0.25 VMO, 0.125 VMO. High-resolution XPS spectra of (d) Mn 2p, (e) O 1s, (f) V 2p of 0.5 VMO.

XPS provides a sensitive measurement of the chemical state in the near surface region of materials. It was carried out on the compounds to confirm the presence of element V and identify the MnO_2 structure. Fig. 2d-f depicted the binding energy of 0.5 VMO corresponding to the Mn 2p, O 1s and V 2p, respectively. It can be observed that the Mn $2p_{3/2}$ peak centered at around 642 eV while the Mn $2p_{1/2}$ peak at 653.8

eV with a spin-energy separation of 11.8 eV, which agrees well with those reported for MnO_2.[14] The O 1s can be deconvoluted into three peaks, corresponding to Mn-O-Mn (529.4 eV), Mn-O-V (529.9 eV) and Mn-O-H (531.1 eV) which was consistent with previous report. Compared with the sample 0.125 VMO and 0.25 VMO (Figure S5), the peaks of Mn-O-Mn and V 2p shifted to a higher value along with the increasing content of V. The higher binding energy indicated that V doped MnO_2 nanosheets have more stable structure and clearly suggested the incorporation of V into the MnO_2 lattice.[15]

The Fourier Transform Infrared (FT-IR) spectroscopy can yield a more complete and reliable description for materials due to their sensitivity to local structures. The FT-IR spectrum of V doped MnO_2 nanosheets were shown in Fig. 3a-b, which displayed similar features as those previously reported for MnO_2 based materials.[13] The broadband at about 3440 cm^{-1} and 1633 cm^{-1} are diagnostic of stretching and bending vibrations of H_2O. The split bands at frequency between 400 cm^{-1} and 800 cm^{-1} were attributed to Mn-O band, the magnifying spectrum showed the infrared absorption bands of 0.5 VMO which slightly shifted to higher wave numbers. This result also illustrated that partial V^{5+} in the reaction solution has entered into MnO_2 lattice.[16]

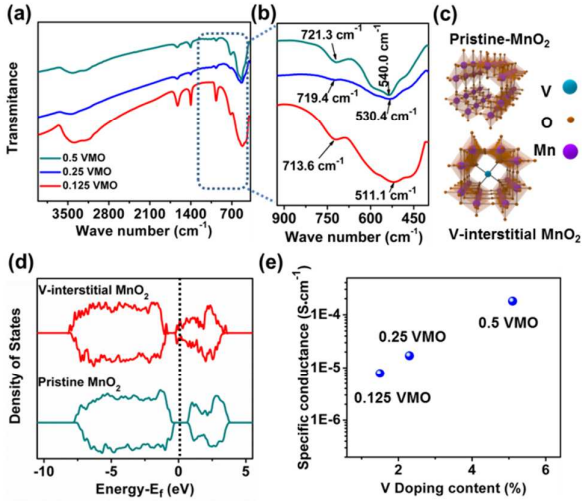

Fig. 3 (a) FTIR spectrum of 0.5 VMO, 0.25 VMO and 0.125 VMO. (b) The peaks between 400 cm^{-1} and 920 cm^{-1} in the FTIR spectrum. (c) Structures of pristine MnO_2 and interstitial V doped MnO_2 model. Blue balls, orange balls, violet balls stand for V, O, Mn atoms, respectively. (d) Density of states of pristine MnO_2 and interstitial V doped MnO_2. (e) Electrical conductivity of 0.5 VMO, 0.25 VMO and 0.125 VMO tested by four-point probe method.

All of the characterizations above indicated that we have synthesized V doped MnO_2 nanosheets successfully. To investigate the influence by V doping, the first principle calculations were employed, and used a 1 × 1 × 3 periodic supercell of α-MnO_2 to carry on the discussions. The model of V-interstitial α-MnO_2(Fig. 3c) was employed to study the density of states (DOS) changes of α-MnO_2 (Fig. 3d). It can be found that the Fermi energy lever of α-MnO_2 increases and moves to the conduction-band minimum (CBM) with V doping. Also, the band gaps are narrowed down as the generating of impurity peaks within the band gap. Accordingly, the electrical conductivity of MnO_2 would be improved from introduction of V. To verify the simulation, the electronic conductivity of these samples was measured using a four-point probe method (Fig. 3e). The tendency of the conductivity change agrees well with V doping content upon these samples.

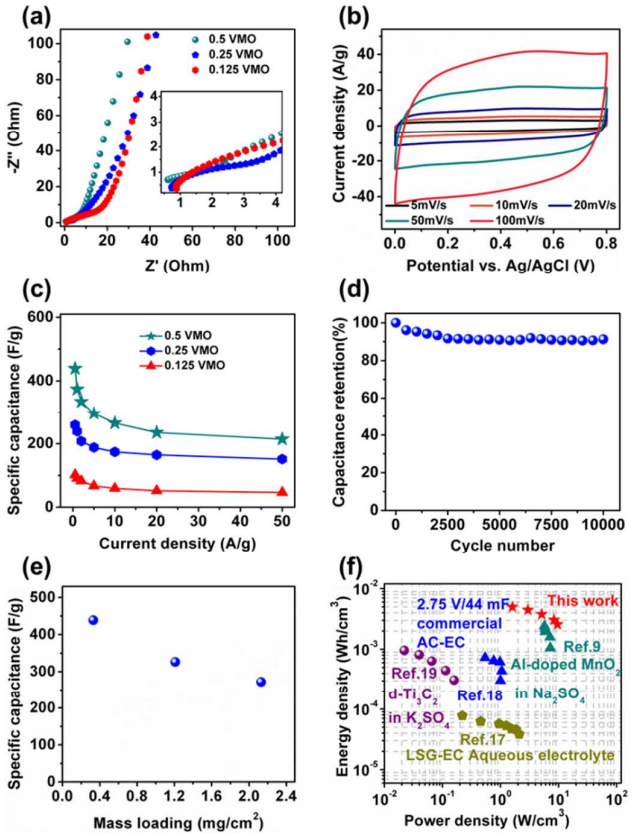

Fig. 4 Electrochemical performance of the electrode materials. (a) EIS analysis of 0.5 VMO, 0.25 VMO, 0.125 VMO. (b) CV curves of 0.5 VMO at scan rate increase from 5 mV/s to 100 mV/s by a typical three-electrode configuration. (c) Gravimetric capacitance as a function of current density for 0.5 VMO, 0.25 VMO and 0.125 VMO. (d) Cycling performance of 0.5 VMO electrode (at a current density of 5 A/g). (e) Gravimetric capacitance of 0.5 VMO under different mass loading. (f) Ragone plot of the device compared with commercial AC-EC,[19] LSG-EC aqueous electrolyte,[20] d-Ti_3C_2 in K_2SO_4[21] and Al-doped MnO_2 in Na_2SO_4.[11]

Generally, the electrochemical performance mainly depends on the specific surface areas and/or electrical conductivity of the electrode, hence 0.5 VMO hold great potential for high performance supercapacitors. Cyclic voltammetry (CV) and galvanostatic charge-discharge (GCD) were carried out to study the electrochemical performances of V doped MnO_2 conducted in a three-electrode configuration with 0.5 M Na_2SO_4 as electrolyte. Electrochemical impedance spectroscopy (EIS) measurement was also conducted to evaluate the difference of electrochemical activity of V doped MnO_2. As depicted in Fig. 4a, the diameter of the semicircle at the high frequency region of these three samples decreased from 18 Ω (0.125 VMO) to 1.5 Ω (0.5 VMO), demonstrating the

less charge-transfer resistance of 0.5 VMO. This result matches well with the electrical test by a standard four-point probe configuration. Fig. 4b showed the typical CV curves of 0.5 VMO at scan rates from 5 mV/s to 100 mV/s. The nearly rectangular shape suggests the great reversible capacitive behavior. The symmetric GCD curves (Fig. S6a) of 0.5 VMO collected at various current densities revealed good coulombic efficiency and reversible ion adsorption/reaction. As a comparison, CV curves of0.125 VMO and 0.25 VMO (Fig. S6b) were also tested under the same condition. The CV curve of 0.5 VMO at sweep rate of 50 mV/s has much larger integral area than the CV curves of 0.125 VMO and 0.25 VMO at same sweep rate, revealing the better specific capacitance (Fig. S6b). 0.5 VMO shows the highest specific capacitance of 439 F/g (195 F/cm^3 and 141 mF/cm^2) at the current density of 0.5 A/g with a good capacitance retention (50.4 %) from 0.5 A/g to 50 A/g, which is almost four times of the capacitance of 0.125 VMO (102 F/g) and 1.7 times of 0.25 VMO (254 F/g). Cycling performance is another key factor in determining electrodes for many practical applications. Generally, the fading in the capacitance of MnO_2–based electrode upon electrochemical cycling results from loss of active materials through partial dissolution of MnO_2 or conversion to electrochemically irreversible species such as Mn_2O_3 and Mn_3O_4. Surprisingly, the cycling performance of 0.5 VMO (Fig. 4d) maintained an excellent capacitance retention of 92 % after 10,000 cycles under the current density of 5 A/g, which is also much better than most of previous reports, such as cobalt-doped MnO_2 hierarchical yolk-shell spheres (90 % after 1,000 cycles),[17] carbon nanotube/MnO_2 hybrid ultrathin film (88.4 % after 1,000 cycles),[14] and α-MnO_2 sphere (70 % after only 500 cycles),[7] demonstrating the electrochemical stability of the V doped MnO_2 nanosheets. The specific capacitance of V doped MnO_2 with different mass loading were also investigated (Fig. 4e). The specific capacitance of 0.5 VMO reached to 272 F/g even at a mass loading of 2.13 mg/cm^2. This value is superior to most reported MnO_2-based ECs.[17,18] The high performance of V doped α-MnO_2 is mainly ascribed to these following features: (I) 2D structure would offer large electrochemically active surface areas for charge transfer and reduced ion diffusion length during the charge/discharge process; (II) the high conductivity of 0.5 VMO facilitates easily access of electron transport through the whole electrode.

To evaluate the potential of 0.5 VMO for energy storage under real conditions, two-electrode symmetric electrochemical capacitor (SEC) based on these 2D nanosheets was performed using 0.5 M Na_2SO_4 as electrolyte. The rectangular shape CV profiles of the cell in voltage window 0~0.8 V consist with the three electrode testing system (Fig. S7a). GCD curves under different current density (Fig. S7b) exhibited typical symmetrical linear charge-discharge characteristics in a range of 0.21~4.3 A/cm^3, suggesting a highly reversible charge-discharge behavior. The Ragone plots shown in Figure 4f normalized the relationship between the volumetric energy density and power density. The volumetric energy density could deliver a high energy density of 4.98 mWh/cm^3 at a power density of 1.6 W/cm^3, which higher than many works.[11, 19-21]

4. Conclusion

In summary, V doped α-MnO_2 nanosheets were synthesized hydrothermally by using a certain amount of V dopant. It should mentioned that we have simplified the synthesis methods of 2D electrode materials, moreover, in the formation process of 2D MnO_2, V doped into the (2 × 2) tunnels simultaneously. Thus the intentionally doping modification could efficiently enlarge the specific surface areas and enhance electronic conductivity. Hence render the V doped α-MnO_2 nanosheets with high specific capacitance (439 F/g, 195 F/cm^3 and 141 mF/cm^2), good rate capability (50.4 % retention from 0.5 A/g to 50 A/g) and remarkable cycling performance (92 % maintained after 10,000 cycles under 5 A/g). All the results demonstrated vanadium modification being an effective and convenient technique to tailor the morphology and improve the electrochemical performance of manganese dioxides-based supercapacitors, and should be applicable to a wide range of energy storage electrode materials such as MoO_3, Nb_2O_5, WO_3 and other metal oxides.

Acknowledgements

This work was financially supported by the National Natural Science Foundation of China (51322210, 61434001), Director Fund of WNLO, and the China Postdoctoral Science Foundation (2014M550390). The authors thank Dr. J. Su for the help in TEM experiments, and Dr. Z. F. Li and Prof. Y. H. Zhou for their help in resistance measurement. The auothors also thank the Analysis and Testing Center of Huazhong University of Science and Technology.

Reference

1 C. Xu, F. Kang, B. Li, H. Du, *J. Mater. Res,* 2010, **25**, 1421-1432.
2 B. S. Yin, S. W. Zhang, H. Jiang, F.Y. Qu, X. Wu, *J. Mater. Chem. A,* 2015, **3**, 5722-5729.
3 K. Zhang, X. Han, Z. Hu, X. Zhang, Z. Tao, J. Chen, *Chem. Soc. Rev,* 2015, **44**, 699-728.
4 Z. Yu, L. Tetard, L. Zhai, J. Thomas, *Energy Environ. Sci,* 2014, DOI: 10.1039/C4EE0329B.
5 Y. Liu, Y. Jiao, B. S. Yin, S. W. Zhang, F.Y. Qu, X. Wu, *J. Mater. Chem. A,* 2015, **3**, 3676-3682.
6 M. Nakayama, K. Suzuki, K. Okamura, R. Inoue, L. Athouël, O. Crosnier, T. Brousse, *J. Electrochem. Soc,* 2010, **157**, A1067-A1072.
7 S. Devaraj, N. Munichandraiah, *J. Phys. Chem. C,* 2008, 112, 4406-4417.
8 J. Zhu, Q. Li, W. Bi, L. Bai, X. Zhang, J. Zhou, Y. Xie, *J. Mater. Chem. A,* 2013,**1**, 8154-8159.
9 G. Zhao, J. Li, L. Jiang, H. Dong, X. Wang, W. Hu, *Chem. Sci,* 2012, **3**, 433-437.
10 L.T. Tseng, Y. Lu, H. M. Fan, Y. Wang, X. Luo, T. Liu, P. Munroe, S. Li, J. Yi, *Sci. Rep,* 2015, DOI: 10.1038/srep09094.

11 Z. M. Hu, X. Xiao, C. Chen, T. Q. Li, L. Huang, C. F. Zhang, J. Su, L. Miao, J. J. Jiang, Y. R. Zhang, J. Zhou, *Nano Energy,* 2015, **11**, 226-234.
12 S. Cheng, L. Yang, D. Chen, X. Ji, Z.-j. Jiang, D. Ding, M. Liu, *Nano Energy,* 2014, **9**, 161-167.
13 T. Gao, M. Glerup, F. Krumeich, R. Nesper, H. Fjellvåg, P. Norby, *J. Phys. Chem. C,* 2008, **112**, 13134-13140.
14 S. W. Lee, J. Kim, S. Chen, P. T. Hammond, Y. Shao-Horn, *ACS nano,* 2010, **4**, 3889-3896.
15 W.H. Ryu, D.W. Han, W.K. Kim, H.S. Kwon, *J. Nanopart. Res,* 2011, **13**, 4777-4784.
16 J. Zeng, S. Wang, J. Yu, H. Cheng, H. Tan, Q. Liu, J. Wu, *J. Solid State Electr,* 2014, **18**, 1585-1591.
17 C. L. Tang, X. Wei, Y. M. Jiang, X. Y. Wu, L. N. Han, K. X. Wang, J.S. Chen, *J. Phys. Chem. C,* 2015, **119**, 8465-8471.
18 G. Yu, L. Hu, N. Liu, H. Wang, M. Vosgueritchian, Y. Yang, Y. Cui, Z. Bao, *Nano lett,* 2011, **11**, 4438-4442.
19 M. F. El-Kady, V. Strong, S. Dubin, R. B. Kaner, *Science,* 2012, **335**, 1326-1330.
20 W. Xiao, H. Xia, J. Y. H. Fuh, L. Lu, *J. Electrochem. Soc,* 2009, **156**, A627-A633.
21 M. R. Lukatskaya, O. Mashtalir, C. E. Ren, Y. Dall'Agnese, P. Rozier, P. L. Taberna, M. Naguib, P. Simon, M. W. Barsoum, Y. Gogotsi, *Science,* 2013, **341**, 1502-1505.